JOURNAL OF CATALYSIS 103, 407–418 (1987)

Synthesis, Characterization, and Catalytic Activity of $LaRhO_3$

H. J. GYSLING, J. R. MONNIER, AND G. APAI

Corporate Research Laboratories, Eastman Kodak Company, Rochester, New York 14650

Received April 18, 1986; revised September 23, 1986

Lanthanum rhodate, $LaRhO_3$, has been prepared by high-temperature reaction of the nitrates, prepared *in situ* from the corresponding oxides. Use of a slight excess of the rare-earth oxide, and removal of this component from the product with a warm, dilute acetic acid leach, provided the pure perovskite. The presence of pure monophasic material was confirmed by X-ray diffraction and X-ray photoelectron spectroscopy (XPS). Comparison of the material made with a slight excess of the rare-earth oxide to a sample prepared using a slight excess of Rh_2O_3 showed that the excess Rh_2O_3 cannot be removed by leaching. These studies demonstrate the need for careful attention to the synthetic method used for the preparation of solid-state materials which are to be evaluated as catalysts, and the utility of XPS for monitoring the purity of such materials. Temperature-programmed reduction and XPS studies of $LaRhO_3$ have shown that, contrary to claims in the literature, no stable Rh^+ species are observed on heating this material in pure H_2 or 1 : 1 H_2 : CO, although in the latter case some stabilization of the original perovskite is observed vs reduction in pure H_2. The activity of $LaRhO_3$ as a catalyst for the formation of linear alcohols from syn gas (i.e., 1 : 1 H_2 : CO), as well as for ethylene hydroformylation, is also reported. The results imply that oxygenate formation occurs on Rh^0 centers and that the temperature-dependent competition between associative and dissociative CO adsorption on Rh^0 is the major factor in selectivity distributions.

I. INTRODUCTION

Metallic rhodium, rhodium oxides, and Rh-containing mixed-oxide catalysts have been extensively studied (*1–8*) for Fischer–Tropsch activity and their ability to produce different distributions of oxygenated products. Ichikawa and co-workers (*1, 2*) have correlated X-ray photoelectron spectroscopy (XPS) measurements of supported Rh catalysts with their corresponding Fischer–Tropsch oxygenate distributions and concluded that, for selective C_2-oxygenate formation, both Rh^0 and Rh^+ sites were required. They proposed that Rh^0 sites functioned as CO dissociation sites in the formation of alkyl groups, while Rh^+ served as the site for associative CO adsorption and subsequent CO insertion to form acyl species. Similarly, Wilson *et al.* (*3*) have concluded that the stabilization of Rh^+ by Mn promoters in silica-supported Rh catalysts may be responsible for the enhanced C_2-oxygenate selectivity under syn gas reaction conditions.

Somorjai and co-workers (*4–6*), using a different approach, have studied the syn gas activity of clean and oxidized Rh foil (*4*), anhydrous and hydrated rhodium oxide (i.e., Rh_2O_3 and $Rh_2O_3 \cdot 5H_2O$) (*5*), and $LaRhO_3$ (*6*) at different temperatures and, presumably, at different levels of reduction. They also concluded that for the selective C_2 and C_2^+ oxygenate formation to occur efficiently, Rh^0 and Rh^+ are required for facile CO dissociation and CO insertion, respectively.

Thus, there are strong implications as to the importance of the oxidation state of rhodium in controlling the linear oxygenate selectivity and product distribution in syn gas transformations (*7*).

The present investigation was aimed at the evaluation of the importance of the oxidation state of Rh-based catalysts which are of use for the conversion of syn gas to

0021-9517/87 $3.00

linear alcohols and for the hydroformylation of olefins. The Rh system we have chosen is $LaRhO_3$. Specifically, we have investigated in some detail the synthesis, characterization, and catalytic activity of lanthanum rhodate, $LaRhO_3$, with an emphasis on the identification of the oxidation states of the rhodium under different reaction conditions. When appropriate, comparison will be made with a conventional Rh/SiO_2 catalyst prepared by impregnation techniques.

II. EXPERIMENTAL

A. Catalyst Preparation

1. Synthesis of the Rare-Earth Rhodates

Starting materials. La_2O_3 and $Rh_2O_3 \cdot 5H_2O$ were obtained from Strem Chemicals, Inc. $Rh(NO_3)_3$ was obtained from Alfa Products. Rh_2O_3 was obtained from Aesar (Johnson Matthey, Inc.).

Lanthanum oxalate ($La_2(C_2O_4)_3 \cdot 12H_2O$) preparation. Commercial La_2O_3 was dissolved in concentrated HNO_3 and the solution was filtered to remove any particulate matter. Ammonium hydroxide (1 : 1) was added to the solution until the first faint white precipitate appeared, at which point an excess of 1 *M* ammonium oxalate was added. The resulting precipitate was decomposed in air to the oxide (La_2O_3) and, from the weight loss, the formulation $La_2(C_2O_4)_3 \cdot 12H_2O$ was assigned to the product.

a. $LaRhO_3$ (first preparation). $La_2(C_2O_4)_3 \cdot 12H_2O$ (1.5920 g, 2.1 mm) and $Rh_2O_3 \cdot 5H_2O$ (0.6878 g, 2.0 mm) were ground well in an agate mortar and added to a Pt crucible. Concentrated nitric acid was added dropwise to a give a paste. The crucible was then covered, placed in a fire-brick holder, and heated overnight at 150°C in a drying oven. The dried sample was then heated in a Harper furnace at 1000°C in air for 24 h. An X-ray diffraction (XRD) pattern of this product was recorded and the product was then ground well in an agate mortar and refired for 24 h at 1000°C. No change in the XRD pattern was observed after the second firing. The black product was then leached with 3 × 150-ml portions of 50°C, 20% acetic acid, washed well with water and acetone, and dried overnight over P_2O_5 in a vacuum desiccator. The product was characterized as pure $LaRhO_3$ by powder XRD (Fig. 1A).

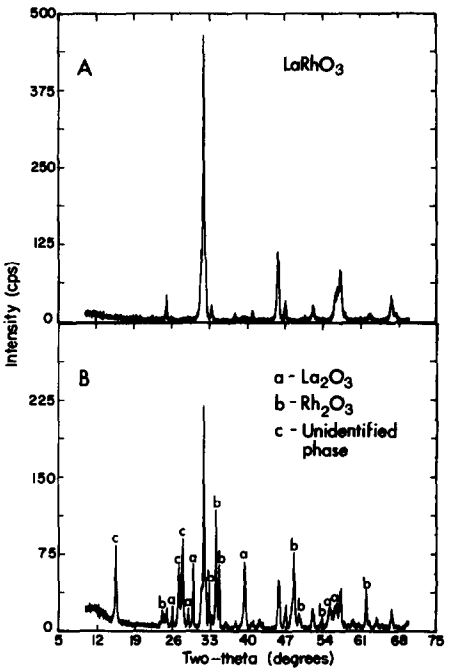

FIG. 1. Powder XRD pattern of (A) monophasic $LaRhO_3$; (B) $LaRhO_3$ prepared from the oxides at 1100°C. The additional impurity phases found in this preparation are a, La_2O_3; b, Rh_2O_3; c, unidentified phase.

The Pt crucible was cleaned between runs using a potassium pyrosulfate flux, followed by washing with boiling dilute HCl and then distilled water.

b. $LaRhO_3$ (second preparation). Stoichiometric amounts of dried La_2O_3 and $Rh_2O_3 \cdot 5H_2O$ were ground in an agate mortar and heated in a Pt crucible for 24 h at 1100°C to give a gray-black powder. This procedure (i.e., that of Ref. (*6*)) gives a product characterized by powder XRD as a mixture of $LaRhO_3$, La_2O_3, Rh_2O_3, and an unidentified phase (Fig. 1B).

2. Synthesis of Silica-Supported Rhodium

The Rh/SiO_2 catalyst was prepared by the impregnation of an aqueous solution of $Rh(NO_3)_3$ onto Davison grade 59 SiO_2 (250 m^2/g). After drying at 120°C, the catalyst was activated in 1 atm of flowing H_2 at 250°C for 4 h prior to the catalytic evaluation. Elemental analysis of the catalyst by atomic absorption gave a Rh loading of 1.5% by weight. Characterization of the catalyst by H_2 chemisorption showed the Rh to be present as crystallites with an average diameter of 34 Å.

3. Synthesis of Powdered Metallic Rhodium

Rh_2O_3 powder was reduced in flowing H_2 at 400°C for 4 h *in situ* prior to catalytic evaluation to prevent surface oxidation from air exposure.

B. Characterization Methods

1. XRD

The powder XRD patterns were recorded as packed slides with a Philips diffractometer using monochromatized high intensity Cu$K\alpha$ radiation (λ = 1.5405 Å). The patterns were recorded from $30° \leq 2\theta \leq 70°$ with a scan rate of 1° (2θ)/min and a chart speed of 30 in./h. Cell parameters were determined by a least-squares refinement of the reflections. Programs for conversion of the 2θ values to d spacings and calculation of the cell parameters were written by Kirby Dwight of the Materials Research Laboratory at Brown University.

2. Temperature-Programmed Reduction (TPR)

The TPR technique was a dynamic one in which ultrapure H_2 (99.99% purity prepared by diffusion through a Pd thimble) (RSD-50 hydrogen purifier) at 90 ml (STP)/min was used as a sweep/reducing gas to transfer H_2O (formed during the reduction of the oxide) into the differentially pumped inlet system of a UTI Q-30C mass spectrometer system. All stainless-steel transfer lines were maintained at greater than 100°C to prevent condensation of H_2O in the sweep stream. The intensity of the H_2O^+ signal was monitored and stored in the memory of a UTI 2054 programmable peak selector.

The thermocouple used to measure the temperature of the sample during reduction was imbedded in the sample using a Pyrex thermowell. The thermocouple output was amplified as a 0- to 10-V signal and was stored along with the H_2O^+ peak intensity data in the programmable peak selector. In practice, the H_2O^+ intensity values and corresponding temperatures were scanned and stored in memory every 1–2 sec during the course of the TPR experiment.

The temperature programmer was a Theall TP-2200 programmer connected to a small 1500-W nichrome-wrapped quartz furnace that was fabricated in-house. The dimensions of the furnace and the calibration of the programmer gave linear heating rates up to 60°C/min. The TPR experiments in this study were conducted at 10°C/min.

3. X-ray Photoelectron Spectroscopy

XPS measurements were made with unmonochromatized Mg$K\alpha$ radiation ($h\nu$ = 1253.6 eV) using a Vacuum Generators ESCALAB Mark II spectrometer system in constant analyzer energy mode corresponding to 0.2 eV resolution. Pressure of the vacuum chamber during measurement was 1×10^{-9} mbar. Binding energies for selected peaks of $LaRhO_3$ were determined on the untreated material by assigning the C 1s peak of the adventitious carbon to be 284.6 eV. Thereafter, the perovskite peaks could be used as a secondary reference. This procedure yielded identical positions for Rh^{3+} in $LaRhO_3$ before and after low-temperature hydrogen reductions, and yielded the commonly accepted binding energy values for Rh^0 upon severe reduction (307.0 eV).

Samples for surface analysis were identical to those used in the other physical studies in this work. Pressed pellets were formed under ca. 1 ton pressure to fit into a

stainless-steel sample holder. Reduction treatments were done in a high-pressure gas cell attached directly to the ultrahigh vacuum (UHV) chamber (typical conditions): 1 atm hydrogen flowing at 30 SCCM at temperatures between 100 and 350°C).

C. Catalytic Evaluation Techniques

All catalytic activity measurements were conducted in a single-pass high-pressure flow reactor. Analyses of reactor effluent were made using an in-line gas sampling loop which was directly plumbed to a Varian 3760 gas chromatograph. Separation and quantitative analysis of all the reaction products were made using a packed Chromosorb 102 column and flame ionization detection.

The reaction conditions for Fischer–Tropsch syntheses were 800 psig overall pressure and a feed composition of $H_2 : CO = 1 : 1$. The reactor temperatures ranged from 220 to 350°C for $LaRhO_3$ and 225–440°C for Rh/SiO_2. In all cases, CO conversion levels were maintained at ca. 3%. For reaction temperatures of 375 and 400°C, lower catalyst loadings were required. In order to determine whether equilibrium conversion levels were attained at reaction temperatures, thermodynamically allowed rates of formation of CH_3OH and C_2-oxygenates were calculated for reaction temperatures of 325°C or higher. In all instances, the experimentally observed rates of formation were far below those permitted at thermodynamic equilibrium, indicating the rates of formation were kinetically, and not thermodynamically, controlled. The gas phase hydroformylation of C_2H_4 was carried out at 150°C, 250 psig overall pressure, and a feed composition of $C_2H_4 : H_2 : CO = 1 : 1 : 1$.

III. Results and Discussion

A. Synthesis of Rare-Earth Rhodates

$LaRhO_3$ has been previously prepared by the reaction of stoichiometric amounts of La_2O_3 and Rh_2O_3 in a Pt crucible at 1000 to 1100°C (*8–10*). As is the general practice in such solid-state reactions, the materials are heated for 24 h, cooled, ground well in a mortar, and refired for another 24 h. Completion of the reaction is monitored by powder XRD after each firing. An added complication in the case of such rhodium perovskites is the insolubility of the high-temperature form of Rh_2O_3 which requires that the synthesis of pure phase be carried out using a slight excess (ca. 5%) of the rare-earth oxide that can be readily removed after completion of the reaction by leaching with warm 20% acetic acid. Careful attention to this synthetic consideration is critical if such materials are to be evaluated as catalysts, since the presence of excess Rh_2O_3 would result in the facile reduction of this oxide to rhodium metal under the reducing conditions of syn gas transformations.

$LaRhO_3$ was prepared by a modification of the original procedure (*8*) which has been recently reported for the synthesis of $YRhO_3$ (*9, 10*). In this procedure, a mixture of the appropriate oxides or oxalates (5% excess La_2O_3 over the 1 : 1 stoichiometry) in a Pt crucible is converted to a homogeneous mixture of the nitrates by dropwise addition of concentrated nitric acid. When a paste is obtained, the crucible is heated overnight in a 150°C oven and then fired for 24 h at 1000°C. The reaction is complete after one 24-h firing as evidenced by the powder XRD pattern compared to the corresponding pattern after an additional 24-h firing. The surface area of the product is ca. 1 m^2/g, a value generally found for materials prepared in this temperature range. Figure 1A shows the resulting XRD pattern for $LaRhO_3$. Preparation of the perovskite by the procedure of Ref. (*6*) (i.e., heating a mixture of La_2O_3 and $Rh_2O_3 \cdot 5H_2O$ to 1100°C for 24 h) gave a product contaminated with La_2O_3 and Rh_2O_3 (Fig. 1B).

B. Temperature-Programmed Reduction

TPR has previously been shown in this

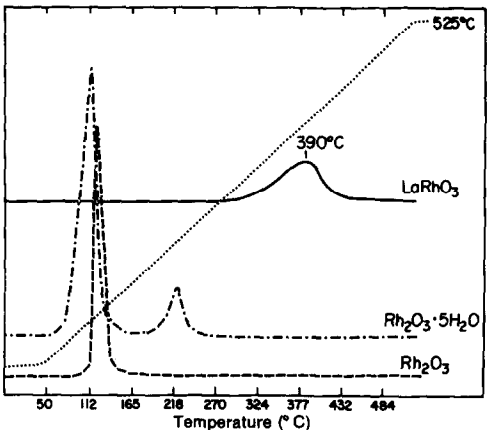

FIG. 2. TPR scans of $LaRhO_3$, $Rh_2O_3 \cdot 5H_2O$, and Rh_2O_3.

laboratory to be a very effective probe of the thermal stability of metal oxide phases (*11*). In general, this technique gives better resolution than thermal gravimetric analysis in following complex reductive decomposition of such materials (*11*). The reductive stability of lanthanum rhodate is illustrated by its TPR scan (Fig. 2). The stability of the oxidized rhodium is significantly enhanced when present in the perovskite lattice (i.e., H_2O peak at 390°C). The TPR scan of an anhydrous Rh_2O_3 sample gave an extremely sharp H_2O peak centered at 120°C, while that for $Rh_2O_3 \cdot 5H_2O$ gave two H_2O peaks centered at 115 and 220°C. The reduction temperature for an unspecified form of rhodium oxide has been reported to be 177°C (*12*).

The stability order of Rh^{3+} oxides, $LaRhO_3 > Rh_2O_3 \cdot 5H_2O > Rh_2O_3$, is in agreement with that of Watson and Somorjai (*5*, *6*). However, the stability limit of $Rh_2O_3 \cdot 5H_2O$ in this study (less than 250°C as evidenced by the TPR scan in Fig. 2) is considerably lower than that claimed by Watson and Somorjai (*5*) who state that $Rh_2O_3 \cdot 5H_2O$ is resistant to reduction to Rh^0 under several hours of syn gas reaction conditions of 300°C, $H_2:CO = 1:1$, and total pressure = 6 atm.

The TPR scan for $LaRhO_3$ indicates that reduction to Rh^0 occurs in a single step. This observation is in excellent agreement with that of Tascon *et al.* (*13*) who used microgravimetric methods to study the temperature-programmed reduction of $LaRhO_3$. These authors found that for a temperature ramp rate of 4°C/min the reduction of $LaRhO_3$ began at about 200°C and passed through a maximum rate of reduction at approximately 425°C. From the TPR curve shape and powder X-ray diffraction analyses at different stages of reduction, Tascon *et al.* (*13*) concluded that the reduction of $LaRhO_3$ occurred in a single step and that rhodium existed in no stable oxidation states between 3+ and 0.

As Gentry *et al.* (*14*) have observed, the reductive stability is also dependent on the pressure of the reducing medium. For example, under Fischer–Tropsch reaction conditions used in this study (800 psig of $H_2:CO = 1:1$), the TPR peak would be shifted to a lower temperature. The extent of this shift can be calculated using the kinetically dependent Arrhenius relationship described by Gentry *et al.* (*14*). Using the activation energy of 30.6 kcal/mole for $LaRhO_3$ reduction determined by Tascon *et al.* (*13*), we calculate that the TPR peak for H_2O formation would be shifted from 390°C at 1 atm of H_2 to approximately 299°C under the reaction conditions used in this study. Thus, reaction temperatures above 300°C should give catalytic activity that reflects the highly reduced state of Rh^0.

Powder XRD of the sample of $LaRhO_3$ (Fig. 1A) subjected to TPR showed only broad peaks due to La_2O_3 and small crystallites of Rh^0 (Fig. 3).

C. X-RAY PHOTOELECTRON SPECTROSCOPY

The range of binding energies reported for various oxidation states of rhodium is ca. 3.9 eV (Table 1). As illustrated from these data, the characterization of the 3+, 1+, and 0 oxidation states of rhodium appears to be possible. The Rh $3d_{5/2}$ binding energy for clean surfaces of rhodium metal is generally accepted to be 307.1 ± 0.1 eV. Binding energies for higher oxidation states

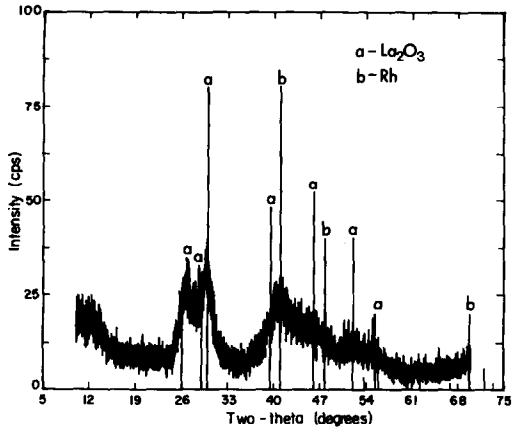

FIG. 3. Powder XRD pattern of the TPR product of $LaRhO_3$ (i.e., La_2O_3 + Rh^0).

of Rh are rather scattered, so only the general ranges of values reported for Rh^+ and Rh^{3+} are listed along with data for a few typical compounds. The Auger parameter for rhodium (*15*) may also be of value in assigning the proper oxidation state; however, these parameters show a significant amount of scatter.

With these facts in mind, we studied a carefully synthesized perovskite, $LaRhO_3$, and have shown that surface monitoring of impurity concentrations is a valuable aid in the synthesis of stoichiometric metal oxides. Additionally, we characterized the surface stability of $LaRhO_3$ under various reduction conditions. Figure 4A illustrates the Rh 3*d* XPS spectrum for $LaRhO_3$ prepared via the *in situ* formation of the nitrates using "stoichiometric amounts" of Rh_2O_3 and La_2O_3. This preparation, although more effective than the ground powder preparative route previously used for catalyst evaluation (*6*), shows the presence of nonstoichiometry at the surface. In Fig. 4A, two sets of Rh 3*d* peaks are readily observed. The most intense $3d_{5/2}$ feature at 308.6 eV is attributable to $LaRhO_3$, while the peak at a higher binding energy (310.5 eV) is most likely attributable to simple Rh_2O_3 based on the XPS binding energy values (Table 1). This slight excess of Rh_2O_3, which is not detected by powder XRD, was introduced in the initial preparation of the nominally "stoichiometric amounts" of lanthanum and rhodium oxides used in the 1100°C firings. At this temperature, the hydrated rhodium oxide is converted into the very insoluble amorphous Rh_2O_3. This latter trace impurity cannot be removed by leaching the product with 20% aqueous acetic and at 70°C. Incorporation of excess La_2O_3 is, therefore, critical to ensure complete consumption of Rh_2O_3 to form the perovskite. The excess La_2O_3 can be readily removed from the final

TABLE 1

XPS Data (Rh $3d_{5/2}$) for Some Typical Rhodium Compounds

Rh compounds	Binding energy (eV)	Reference
Rh^0		
Rh metal	307.1	This work
	307.1	(*16*)
	307.1	(*17*)
	308.5	(*5*)
Rh/C (5%) (vacuum/400°C/2 h)	307.3	(*18*)
Rh^+	307.6–309.6	(*19, 26*)
$\{RhCl(COD)\}_2$	308.7	(*21*)
$\{RhCl(CO)(PPh_3)_2\}$	308.9	(*22*)
$\{Rh(H)(CO)(PPh_3)_3\}$	308.7	(*22*)
Rh^{2+}	308.4–309.3	(*20*)
$Rh(O_2CCH_3)_2$	309.0	(*22*)
$\{RhCl_2(P(C_6H_{11})_3)_2\}$	309.2	(*22*)
Rh^{3+}	308.8–311.3	(*6*)
Rh_2O_3	309.1	(*21*)
	310.0	(*5*)
	310.5	This work
$Rh_2O_3 \cdot 5H_2O$	311.0	(*5*)
$LaRhO_3$	308.6	This work
	311.0	(*6*)
$RhCl_3 \cdot 3H_2O$	310.0	(*22*)
	310.2	(*23*)
	309.7	(*24*)
	310.3	(*21*)
$RhCl_3(PPh_3)_3$	310.2	(*22*)
$\{Rh(NH_3)_5Cl\}Cl_2$	310.2	(*18*)

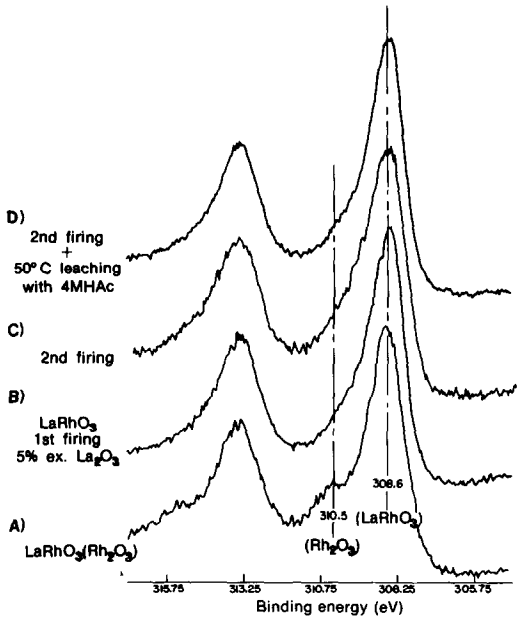

FIG. 4. Rh 3*d* XPS spectra of $LaRhO_3$: (A) $LaRhO_3$ (Rh_2O_3); (B) $LaRhO_3$, 1st firing, 5% extra La_2O_3; (C) 2nd firing; (D) 2nd firing + 50°C leaching with 4 *M* acetic acid.

product by leaching with 20% aqueous acetic acid at 50°C to give monophasic $LaRhO_3$. Figures 4B–D show Rh 3*d* spectra for $LaRhO_3$ prepared in the presence of excess La_2O_3. No additional peak attributable to Rh_2O_3 appears in these spectra. Each of the samples produces the identical binding energy (308.6 ± 0.15 eV) when referred to adventitious carbon.

XPS spectra illustrating the surface stability of $LaRhO_3$ under hydrogen or syn gas reaction conditions are shown in Fig. 5. To illustrate the sensitivity for surface Rh_2O_3 detection under hydrogen reduction, we use the Rh_2O_3-impure perovskite formed from a nominally "stoichiometric" mixture of the simple oxides. Figure 5A again shows the untreated sample containing both Rh_2O_3 and $LaRhO_3$. Upon low-temperature hydrogen reduction, the Rh_2O_3 phase is observed to disappear with the simultaneous formation of Rh^0 characterized by a binding energy of 307.1 eV (Fig. 5B). This binding energy is identical to that of Rh metal and, as such, reflects bulk-like particles supported on an oxide substrate. Similar experiments were performed on the $LaRhO_3$ samples prepared with excess La_2O_3 (i.e., Fig. 4D) to demonstrate that the surface of this perovskite was pure enough to exhibit no detectable Rh_2O_3. Reduction at 250°C in 1 atm of flowing hydrogen was insufficient to completely reduce the surface of $LaRhO_3$ (Fig. 5C). Syn gas reaction conditions tend to promote the stabilization of $LaRhO_3$. Under these conditions, 300°C in a 2:1 = H_2:CO flow at 1 atm total pressure, two peaks are observed which we attribute to Rh^{3+} in $LaRhO_3$ and Rh^0 in reduced metallic particles (Fig. 5D). The full Rh 3*d* spectrum can be produced by summing the separate spectra for untreated $LaRhO_3$ (Rh^{3+}, 308.6 eV) and fully reduced $LaRhO_3$ (Rh^0, 307.1 eV) (see Fig.

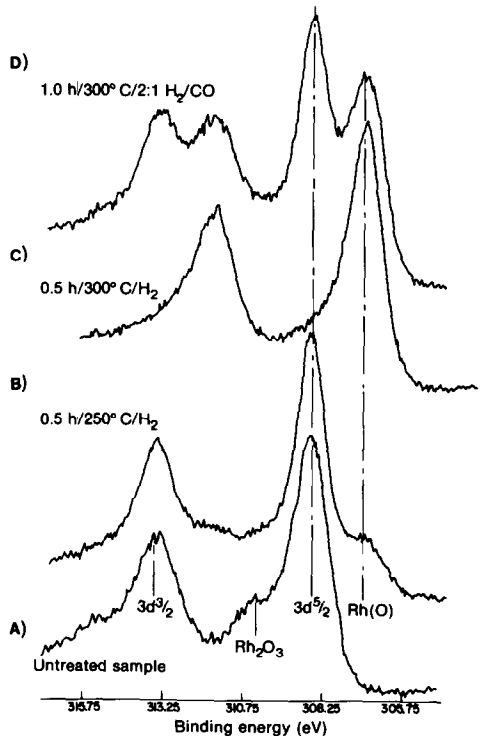

FIG. 5. (A) Rh 3*d* XPS spectra of $LaRhO_3$ (containing trace impurity of Rh_2O_3) and its reduction products on heating in pure H_2; (B) 0.5 h, 250°C; (C) 0.5 h, 300°C; and (D) in 2:1 H_2:CO at 300°C.

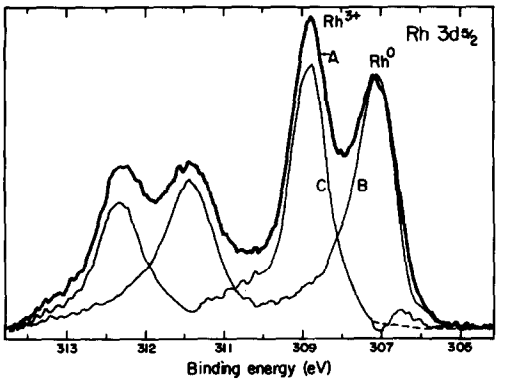

FIG. 6. Deconvolution of the Rh $3d_{5/2}$ spectrum of $LaRhO_3$ reduced at 300°C in 2:1 H_2:CO into Rh^0 and Rh^{3+} components from fully reduced $LaRhO_3$ and untreated $LaRhO_3$.

6). No Rh^+ component in the intermediate region (ca. 308 eV) is apparent.

These results differ from previously reported work (*6*) and must be attributed to the improved synthetic procedure used in this work. Preparation of $LaRhO_3$ using a nominally "stoichiometric" mixture of the oxides (*6*) results in residual Rh_2O_3 as detected by both XRD and XPS. The full width half maximum (FWHM) for the Rh $3d_{5/2}$ peak of $LaRhO_3$ reported previously (*6*) was 2.0 eV, while the binding energy reported was 311.0 eV. We obtain a FWHM of 1.25 eV and a binding energy of 308.6 eV, showing that there is a distinct difference in the surface characteristics. Since the surface properties of a catalyst will control the activity and selectivity of heterogeneous reaction, careful control of sample surface preparation is needed. These new data concerning the surface reduction characteristics can be used in conjunction with kinetic and chemisorption data to offer a new explanation for oxygenate selectivity in rhodium catalysts.

IV. CATALYTIC ACTIVITY

The Fischer–Tropsch activities for $LaRhO_3$ at different reaction temperatures are displayed as Schulz–Flory plots in Fig. 7. At a reaction temperature of 300°C, the formation rates of C_2-oxygenates (CH_3CHO + C_2H_5OH) are greater than for CH_3OH, indicating that the mechanism for CH_3OH formation is different from the mechanism for formation of higher oxygenates. Similar mechanisms for both CH_3OH and higher oxygenates would imply some typical Schulz–Flory growth mechanism and require that the molar rate of CH_3OH formation be greater than the molar rate of C_2-oxygenate formation. Thus, CH_3OH is formed by the reduction of adsorbed CO by a mechanism not containing intermediates common to those by which higher oxygenates are formed. The higher oxygenates are apparently formed by a CO insertion into surface alkyl fragments as others have noted (*1, 5*). Since XPS did not detect any Rh^+ on the $LaRhO_3$ surface following a much milder pretreatment at 300°C and the TPR curve indicated that, in 1 atm of H_2, 50% of the lattice O^{2-} associated with Rh in $LaRhO_3$ had been removed at 400°C, it is

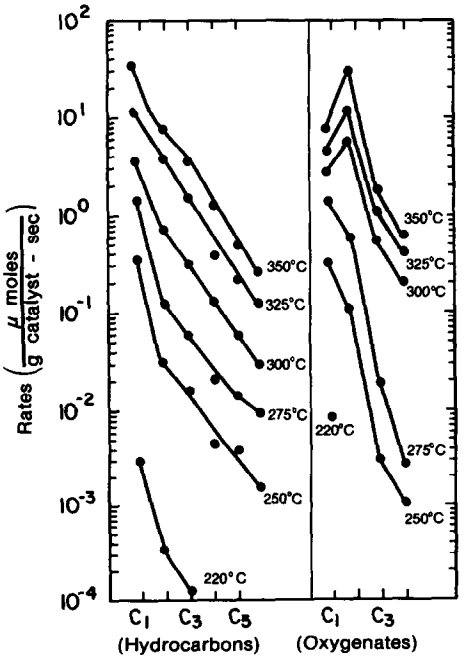

FIG. 7. Fischer–Tropsch activity of $LaRhO_3$ as a function of temperature. Schulz–Flory plots for $LaRhO_3$.

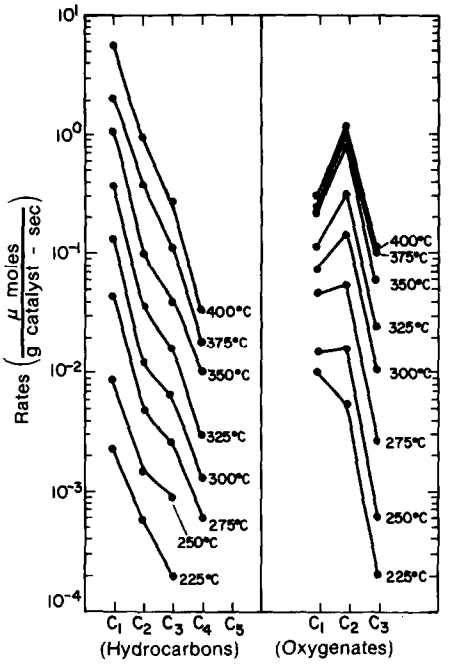

FIG. 8. Fischer–Tropsch activity of Rh/SiO_2 as a function of temperature. Schulz–Flory plots for $LaRhO_3$.

difficult to envision the existence of stable Rh^+ on the catalyst surface under our reaction conditions. Note that the TPR conditions at 400°C correspond to ca. 300°C under the high-pressure reaction conditions.

The above results are strongly corroborated by the data in Fig. 8 which displays the Fischer–Tropsch activity for a conventional Rh/SiO_2 catalyst over the temperature interval 225–400°C. The shapes of the Schulz–Flory curves for $LaRhO_3$ (Fig. 7) and Rh/SiO_2 (Fig. 8) at similar temperatures are essentially indistinguishable, suggesting the same type of catalytically active Rh species for both catalysts. Since the Rh present on such SiO_2-supported catalysts is considered to be zero valent under these reaction conditions (*17, 18, 25*), it is consistent that the active rhodium present in "$LaRhO_3$" is also zero valent.

Other workers have reported similar catalytic behavior for supported Rh catalysts under reduction conditions similar to those used in this study. Bhasin *et al.* (*26*) found that for a 2.5% Rh/SiO_2 catalyst evaluated at 300°C, 1000 psig, and $H_2:CO = 1:1$, the molar selectivity to C_2-oxygenates was approximately 20% while that for CH_3OH was less than 2%. Likewise, Arakawa and coworkers (*27*) observed that the molar selectivities for C_2-oxygenates and CH_3OH were approximately 35 and 3%, respectively, for a 4.7% Rh/SiO_2 catalyst which was tested at 280°C, 700 psig, and $H_2:CO = 1:1$.

In order to test the intrinsic Fischer–Tropsch activity of unsupported Rh^0, a sample of Rh_2O_3 was reduced *in situ* in flowing H_2 at 400°C for 4 h prior to evaluation at 300°C, 800 psig, and $H_2:CO = 1:1$. As the TPR scan in Fig. 2 shows, the Rh_2O_3 undergoes a sharp, single-stage reduction at approximately 120°C. In addition, from the ΔG_f^0 data of Reed (*28*) we can calculate that the reduction by H_2 of Rh_2O_3 to Rh^0 is thermodynamically favorable, even at room temperature. Thus, we can be reasonably certain that the Rh_2O_3 is totally reduced to Rh^0 after 4 h in flowing H_2 at 400°C.

The Fischer–Tropsch activity of the prereduced Rh_2O_3 catalyst is presented in Fig. 9. The shapes of the Schulz–Flory curves for product formation are in general agreement with those for $LaRhO_3$ and Rh/SiO_2. These data indicate that under normal

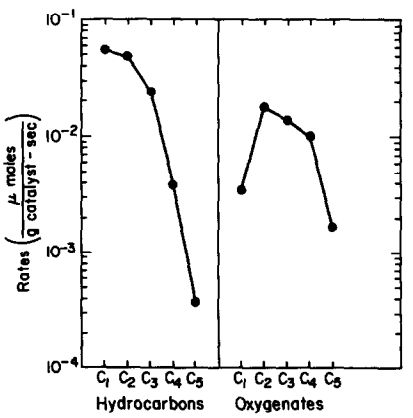

FIG. 9. Fischer–Tropsch activity of Rh_2O_3 following *in situ* reduction at 400°C in flowing H_2 for 4 h. Reaction temperature in 300°C. Schulz–Flory plots for Rh_2O_3.

Fischer–Tropsch conditions Rh^0 produces substantial amounts of C_2–C_5 linear oxygenates (primarily aldehydes). The similarity of the shapes of the Schulz–Flory curves for the C_1–C_4 hydrocarbons with those for the C_2–C_5 linear oxygenates supports the generally accepted view that linear oxygenate formation over Rh catalysts proceeds via CO insertion into Rh–C_n alkyl fragments to form C_{n+1} linear oxygenates.

Further evidence for the role of Rh^0 in controlling the Fischer–Tropsch activity of $LaRhO_3$ under reaction conditions was obtained by measuring the activity of the $LaRhO_3$ catalyst sample following in situ reduction in 1 atm of flowing H_2 at 550°C for 2 h. The shapes of the Schulz–Flory product distribution curves at 250 and 300°C were essentially identical to those at the same temperatures in Fig. 7. The measured rates of product formation were slightly different, however, due to the sintering of the Rh^0 particles at 550°C, which resulted in a lower surface area of Rh^0 sites.

These results suggest there is no need to invoke Rh^+ to explain the high rates of C_2-oxygenate formation. Rather, the poor CO dissociation capability of Rh^0 (*26*) requires higher temperatures to efficiently dissociate CO and form surface alkyl fragments in high enough surface concentrations so that CO insertion into the metal–alkyl bond (to form acyl species) can compete favorably with hydrogenation of adsorbed CO and surface alkyls to form CH_3OH and paraffins, respectively.

As others have noted, Rh^0 surfaces do not readily dissociate CO until higher temperatures are reached. Yates *et al.* (*30*), using UHV techniques, have concluded that CO dissociation does not occur readily over Rh(111) surfaces until $T > 600$°C are attained. Similarly, Gorodetskii and Nieuwenhuys (*31*) concluded that the rate of CO dissociation, at 0.1 Torr of CO pressure on both densely packed and open Rh surfaces, was negligible until temperatures above 700°C were reached.

Under conditions more similar to those of the present study, Solymosi and Erdohelyi (*29*) found that when CO at 1 atm pressure was exposed to a Rh/Al_2O_3 catalyst it did not undergo dissociation to any significant degree until temperatures above ca. 275°C were reached. This observation is in excellent agreement with the results of Monnier and Apai (*11*) for the temperature-programmed desorption/dissociation of CO from a 1.5% Rh/SiO_2 catalyst (same Rh/SiO_2 catalyst as used in the present study; Fig. 8). The desorption of molecular CO occurred over the temperature range 70–260°C as a multiplet of four desorption peaks, while CO_2 (from the disproportionation of adsorbed CO) did not occur until temperatures higher than 250°C were reached; the rate of CO_2 formation passed through a maximum at 300°C.

In recent work, Baetzold and Monnier (*32*) have kinetically modeled the CO insertion mechanism for linear oxygenate formation from syn gas and observed that by lowering the activation energy for CO dissociation (with other parameters held constant), the rate of alkyl chain growth increased dramatically. In such a situation it was possible to very closely reproduce the experimentally obtained Schulz–Flory distribution for both linear oxygenates and hydrocarbons over a Ru/SiO_2 catalyst. Clearly, the rate of chain growth is more critical for Rh than for Ru at a given temperature. For similar rates of alkyl chain growth, considerably higher temperatures are required for Rh catalysts.

One way to test the conclusion that no Rh^+ is present is to evaluate $LaRhO_3$ in a catalytic reaction in which Rh^+ is presumably the species responsible for the selective formation of a given product. The catalytically active species in the hydroformylation of olefins by homogeneous Rh catalysts are reported to be Rh^+ complexes (e.g., $Rh(H)(CO)(PPh_3)_3$, $Rh(Cl)(CO)(PPh_3)_3$ (*33*). Thus, we should expect a heterogeneous catalyst containing some Rh in the 1+ oxidation state to be more selective than one which contains no Rh^+.

TABLE 2

The Hydroformylation of C_2H_4 over $LaRhO_3$ as a Function of H_2 Pretreatment Temperature

H_2 pretreatment temperature[a] (°C)	Rates of formation (moles/g cat./sec)		Molar % selectivity
	C_2H_6	C_2H_5CHO	
200	0.054	0.210	80
250	0.168	0.594	78
325	0.087	0.276	76

[a] Catalyst heated in a high-pressure reactor for 1 h at each temperature before catalytic evaluation.

The data in Table 2 reveal that selectivity to C_2H_5CHO is essentially independent of H_2 pretreatment temperature, implying that Rh^+ is not formed at any of the pretreatment temperatures. The range of H_2 pretreatment temperatures in Table 2 encompasses those used by Watson and Somorjai (6) to form presumably stable, catalytically active Rh^+ centers by the reduction of $LaRhO_3$. Thus, the results for C_2H_4 hydroformylation (Table 2) over $LaRhO_3$ as a function of H_2 pretreatment temperature corroborate the hypothesis that Rh^0 is the only catalytically active Rh species present on the surface, since H_2 pretreatment of a similar catalyst at 300°C gave an XPS spectrum of only Rh^0 (Fig. 5C).

To illustrate that Rh^0 does selectively hydroformylate C_2H_4, a second sample of Rh_2O_3 (see TPR scan in Fig. 2) was reduced *in situ* at 400°C in flowing H_2 for 4 h prior to catalytic evaluation for C_2H_4 hydroformylation under the same conditions as used for $LaRhO_3$. At steady-state reaction conditions the molar selectivity of C_2H_5CHO formation was 72%, in very good agreement with the data of Table 2 for $LaRhO_3$.

The rates of product formation (but not selectivity) in Table 2 do increase as the reduction temperature is raised from 200 to 250°C, which is consistent with a higher level of reduction of $LaRhO_3$ to metallic Rh^0. As the reduction temperature is raised to 325°C, the rates of formation fall, suggesting that aggregation of Rh^0 particles has occurred with subsequent loss of Rh^0 surface area.

V. CONCLUSIONS

The formation of pure monophasic $LaRhO_3$ requires that an excess of the rare-earth oxide be used in the synthesis, since any excess present after the reaction can be readily removed by treatment with warm 20% acetic acid. The presence of any excess rhodium in the reaction leads to the presence of the highly insoluble high-temperature form of rhodium oxide which cannot be removed after the firing. This latter oxide is considerably more susceptible to H_2 reduction than the perovskite, $LaRhO_3$. Use of such materials, therefore, in detailed catalytic studies involving correlation of catalytic activities and selectivities with catalyst oxidation states obtained by XPS measurements requires that careful attention be given to preparative procedures to ensure the formation of monophasic material.

XPS has been shown to be a critical complementary analytical probe to XRD to characterize the purity of solid-state materials that are to be used in catalytic studies. It has also shown that, under typical hydrogen reduction conditions, the surface of $LaRhO_3$ is fully reduced to Rh^0. If the catalyst is run under 2:1 H_2:CO at 1 atm at 300°C, the Rh 3*d* core levels can be successfully deconvoluted into Rh^0 and Rh^{3+} contributions alone. The surface shows no Rh^+ contributions.

TPR has been used to study the reductive stability of $LaRhO_3$. This has shown that the bulk stability of Rh^{3+} is substantially enhanced within the rare-earth perovskite crystalline lattice when compared to the stability of Rh^{3+} in the simple oxide lattice (i.e., Rh_2O_3). However, at temperatures comparable to those used for Fischer–Tropsch evaluation, the TPR curves indicate that reduction of $LaRhO_3$ does occur

and, from the XRD and XPS data, that the reduction product is Rh^0.

Under syn gas reaction conditions, $LaRhO_3$ undergoes reduction to Rh^0 with no evidence of any stable Rh^+ species, as had been previously proposed in the literature.

The higher rates of C_2-oxygenate (i.e., $CH_3CHO + C_2H_5OH$) formation vs CH_3OH above 300°C observed for $LaRhO_3$ can be explained by the poor dissociation capability of Rh^0 which requires high temperatures to efficiently dissociate CO and form surface alkyl fragments in sufficiently high surface concentrations to allow favorable competition of CO insertion into the rhodium–alkyl bond (to form acyl species) vs hydrogenation of adsorbed CO and surface alkyls (to form CH_3OH and paraffins, respectively).

A detailed study of the hydroformylation of ethylene over $LaRhO_3$, as a function of H_2 pretreatment of the catalyst, similarly supports the presence of Rh^0, rather than any Rh^+ species, as the active catalyst.

REFERENCES

1. Ichikawa, A., and Fukushima, T., *Chem. Commun.*, p. 321 (1985).
2. Kawai, M., Uda, M., and Ichikawa, M., *J. Phys. Chem.* **89,** 1654 (1985).
3. Wilson, T. P., Kasai, P. H., and Ellgen, P. C., *J. Catal.* **69,** 193 (1981).
4. Castner, D. G., Blackadar, R. L., and Somorjai, G. A., *J. Catal.* **66,** 257 (1980).
5. Watson, P. R., and Somorjai, G. A., *J. Catal.* **72,** 347 (1981).
6. Watson, P. R., and Somorjai, G. A., *J. Catal.* **74,** 282 (1982).
7. Somorjai, G. A., and Davis, S. M., *CHEMTECH*, p. 502 (1983).
8. Wold, A., Post, B., and Banks, E., *J. Amer. Chem. Soc.* **79,** 6365 (1957).
9. Carreiro, L., Qian, Y.-T., Kershaw, R., Dwight, K., and Wold, A., *Mater. Res. Bull.* **20,** 619 (1985).
10. Carreiro, L., Ph.D. thesis, Brown Univ., 1985.
11. Monnier, J. R., and Apai, G., *Prep. Div. Petrol. Chem. Amer. Chem. Soc.* **31**(2), 239 (1986).
12. Vis, J. C., Van't Blik, H. F. C., Huizinga, T., VanGrondelle, J., and Prins, R., *J. Catal.* **95,** 333 (1985).
13. Tascon, J. M. D., Olivan, A. M. O., Tejuca, L. G., and Bell, A. T., *J. Phys. Chem.* **90,** 791 (1986).
14. Gentry, S. J., Hurst, N. W., and Jones, A., *J. Chem. Soc. Faraday Trans. I* **75,** 1688 (1979).
15. Wagner, C. D., Gale, L. H., and Raymond, R. H., *Anal. Chem.* **51,** 466 (1979).
16. Brinen, J. S., and Malera, A., *J. Phys. Chem.* **76,** 2525 (1972).
17. Foley, H. C., DeCanio, S. J., Tau, K. D., Chao, K. J., Onuferko, J. H., Dybowski, C., and Gates, B. C., *J. Amer. Chem. Soc.* **105,** 3074 (1983).
18. Andersson, S. L. T., and Scurrell, M. S., *J. Catal.* **71,** 233 (1981).
19. Andersson, S. L. T., Watters, K. L., and Howe, K. L., *J. Catal.* **69,** 212 (1981).
20. Nefedov, V. I., Shubochikina, E. F., Kolomnikov, I. S., Baranovskii, I. B., Golubnichaya, V. P., Chubochkin, L. K., Porai-Koshits, M. A., and Vol'pin, M. E., *Russ. J. Inorg. Chem.* **18,** 444 (1973).
21. Contour, J. P., Mouvier, G., Hoogewys, M., and Leclere, C., *J. Catal.* **48,** 217 (1977).
22. Furlani, C., Mattogno, G., Polzonetti, G., Sbrana, G., and Valentini, G., *J. Catal.* **94,** 335 (1985).
23. Andersson, S. L. T., and Scurrell, M. S., *J. Catal.* **59,** 340 (1979).
24. Imanka, T., Kaneda, K., Teranishi. T., and Terassawa, M., in "Proceedings, 6th Int. Congr. Catal., London, 1976," p. 509. Chem. Soc., London.
25. Jackson, S. D., *J. Chem. Soc. Faraday Trans. I* **81,** 2225 (1985).
26. Bhasin, M. M., Bartley, W. J., Ellgen, P. C., and Wilson, T. P., *J. Catal.* **54,** 120 (1978).
27. Arakawa, H., Takeuchi, K., Matsuzaki, T., and Sugi, Y., *Chem. Lett.*, p. 1607 (1984).
28. Reed, T. B., "Free Energy of Formation of Binary Compounds: An Atlas of Charts for High Temperature Chemical Calculations," pp. 1–30. MIT Press, Cambridge, MA, 1971.
29. Solymosi, F., and Erdohelyi, A., *Surf. Sci.* **110,** L630 (1981).
30. Yates, J. T., Jr., Williams, E. D., and Weinberg, W. H., *Surf. Sci.* **91,** 562 (1980).
31. Gorodetskii, V. V., and Nieuwenhuys, *Surf. Sci.* **105,** 299 (1981).
32. Baetzold, R. C., and Monnier, J. R., *J. Phys. Chem.* **90,** 2944 (1986).
33. Evans, D., Yagupsky, G., and Wilkinson, G., *J. Chem. Soc. A*, 2260 (1968); Pruett, R. L., and Smith, J. A., *J. Org. Chem.* **34,** 327 (1969); Hjortkjaer, J., Scurrell, M. S., and Simonsen, P., *J. Mol. Catal.* **6,** 405 (1979).